Eng Int Syst (2022) 4: 269–277

Engineering
Intelligent Systems

Recognition of Defects in TOFD Image Based on HSV Black Color Histogram

Qi Yao[1] **and Dayang Jiang**[2],*

[1] *School of Digital Economy, Changzhou College of Information Technology, Changzhou 213164, China*
[2] *Information Center, Changzhou College of Information Technology, Changzhou 213164, China*

In this paper, a TOFD image defect recognition method based on HSV block color histogram is proposed to address the problems of poor image recognition accuracy and long recognition which are the shortcomings of current methods. The aim is to improve the accuracy of defect recognition in images. Depending on the difference in the shape and gray of various types of defects in the actual image, the average ratio of gray defect to background, the defect perimeter area ratio and the defect symmetry are selected as indicators of defects in TOFD images. The hyperspectral sensor is used to denoise the TOFD image with defect indicators to reduce the influence of noise on the accuracy of the defect-recognition result. According to the denoising result, an image defect recognition model is established based on the HSV block color histogram to obtain image defect information. Experimental results show that the proposed method has higher recognition accuracy, shorter time and clearer defect features when applied to TOFD image defect recognition. The proposed method has certain effectiveness and superiority in image processing.

Keywords: HSV block color histogram, TOFD image, hyperspectral sensor, defect index, denoising

1. INTRODUCTION

In recent years, with the rapid development of computers, computer-based vision technologies such as sparse representation and deep learning have opened up new avenues for image processing research. The great success of natural image recognition and classification has prompted people to trial it in various industries (Shota et al., 2018; Simone et al., 2018). However, currently, relatively few related technologies are being applied to identify defects in TOFD images (Jang and Ahn, 2020; Singh et al., 2019).

Due to the variations in the shape, location, direction and size of the defects, the analysis and evaluation ofthe acquired TOFD images are complex tasks (Quionez et al., 2020). At present, most fields still use manual evaluation methods. These are time-consuming and laborious, since they require technicians to rely on their experience to determine whether there are defects, as well as the number, location and type (Umer et al., 2019). This method has several drawbacks: factors such as the physical or professional capabilities of the technicians can produce inconsistent results (Corti et al., 2020). For example, when different technicians evaluate the same TOFD image, they may obtain different results due to their level of care, time constraints, expertise, etc. In addition, due to the greatly improved efficiency of industrial production, a large number of TOFD images are generated every day, so the workload is huge. The fatigue of technicians could lead them to miss defects and allow substandard products to enter the market, resulting in unpredictable losses (Chakraborty et al., 2018). To solve this problem, Shinomiya and Hoshino (2019) proposed an image recognition method based on a low space complexity codebook. The method uses the codebook method to represent the image as a feature vector, and when multiple local feature frames are used, each local feature fr amework generates a

*Corresponding Author Email: dayang784512@126.com

visual vocabulary. In this process, a codebook with a small memory footprint is required. The experimental results show that this method reduces the computational complexity of the image representation step, and gives the experimental results of the online classifier; however, the accuracy of image recognition is not high, resulting in poor image color block recognition (Shinomiya and Hoshino, 2019; Ali et al., 2019). Aljanabi et al. (2018) proposed and designed a new method to realize image similarity and image recognition. The method uses a combination of information theory and joint histogram. Information theory can accurately predict the relationship between image intensity values, while the joint histogram selects a group of local pixel features to construct a multi-dimensional histogram. This method combines the concept of entropy and a 2D joint histogram of two images. Based on the Shannon and Renyi entropy measures, two information theory similarity measures based on histogram are proposed: SHS and RSM. The method is applied to facial recognition, and involves a similarity measurement based on best-matching and the second-best matching in the facial database. The simulation results show that this method has certain advantages in terms of recognition confidence, but the accuracy of recognition results is not high, and the implementation steps are complex and time-consuming.

In order to improve the accuracy of TOFD image-defect recognition, it is necessary to deeply mine the defect features of the TOFD image, and subsequently denoise the image with defect features; integrate the TOFD image defects, establish a TOFD image defect recognition model based on HSV block color histogram to obtain defect information from the TOFD image, thereby completing the defect-recognition process.

2. TOFD IMAGE DEFECT RECOGNITION METHOD

2.1 Select the Defect Index of TOFD Image

In image recognition, the selection of features is very important. In fact, when using SVM for image classification, the important kernel function is also selected according to the feature selection. Although the gray image histogram is easy to obtain, and the image feature selection based on the histogram has achieved good results in the past, the effect of feature extraction using the histogram of the image as input is not good (Kas et al., 2018). This is because the image library itself has obvious diff erences in the histogram performance, but for the defect images in this article, the grayscale performance is relatively simple, and because the collected defect images may have changes in brightness, it is difficult to use the histogram as the whole Enter to get a good recognition ofthe defect (Itakura and Hosoi, 2020).

Through observation and analysis of the collected defects in images, some other features are found in the gray scale and the morphology. For example, the sizing group is generally lighter in gray scale, and the transition between its edge and the background is relatively slow. The sizing group is oft en very irregular in shape, and most of it has a defective main part, and there are many similar antennae extending from the main body. However, stripes or ink blotches are often darker in gray scale, with obvious borders and a single shape; while noise and ink blotches are often close to circular in shape. According to the difference in morphology and gray scale of various types of defects in the actual image (Kroop et al., 2018; Dai et al., 2018), the following three TOFD image defect indicators have been selected as input features for TOFD image-defect recognition.

(1) Defect to background average gray ratio REG

The ratio of the average gray level of the defect to the background is the average gray level of the image excluding the defect area. The ratio of the average gray level of the defect area to the average gray level of the background area can characterize the gray level characteristics of the defect part to a certain extent, and overcome the interference caused by the difference in overall brightness of different images (Chen and Qi, 2019). In the calculation, the binary image generated by the preprocessing is used as the mask image, and the average gray level of the corresponding area is obtained from the original image. The calculation formula is:

$$REG = \overline{g}_p l \overline{g}_q \tag{1}$$

where $\overline{g}_p$ is the average gray value of the defect area; $\overline{g}_q$ is the average gray value of the image excluding the defect area.

(2) Defect perimeter area ratio PSR

The defect perimeter area ratio can indicate whether the defect tends to be round in shape. The simpler the boundary of the defect and the closer it is to the circle, the smaller is the PSR value; the more complex the boundary, the larger is the PSR value. To a certain extent, the PSR value can distinguish noise from other defects. It is calculated with:

$$PSR = k_m / k_n \tag{2}$$

where k_m is the perimeter of the image defect; k_n is the area of the image defect area; k_m and k_n can be measured by the number of pixels.

(3) Defect symmetry SYM

The defect symmetry is the symmetry at both ends of the image defect area, and is calculated with:

$$SYM = \sum_{i=1}^{k} x_i(k) \tag{3}$$

where $x_i(k)$ is the long axis of the image defect area.

Aft er calculating the above three indicators and adding the 256-dimensional statistical data of the histogram, the total dimension of the input mode is set to 261 dimensions. Since the three calculated indicators are not aligned with the histogram statistical measurement, the 261-dimensional input mode should be normalized to balance the impact of each indicator on the recognition result.

2.2 TOFD image Denoising Based on Hyperspectral Sensor

According to the calculation result of TOFD image defect index, the hyperspectral sensor is used to denoise the TOFD image and provide relevant information for the defect recognition of a TOFD image (Sharan and Moir, 2018). The TOFD image is sparsely represented by three-dimensional DCT to achieve image denoising. The three-dimensional DCT transformation is described by the following formula:

$$F(u,v,w) = (REG + PSR + SYM) \times \frac{c(u)c(v)c(w)}{\sqrt{l \times m \times e}} \times \sum_{i=0}^{l-1}\sum_{j=0}^{m-1}\sum_{z=0}^{e-1} f(i,j,z) \quad (4)$$

where f is the gray value of the TOFD image; i, j, z are the three-dimensional image coordinates; m is the corresponding width of the image; l is the corresponding length of the image; e is the number of band sequences.

The product of $N_1, N_2, \cdots, N_L$ -dimensional column vector and $\psi_{N_1} \otimes \psi_{N_2} \cdots \otimes \psi_{N_L}$ matrix is used to calculate $N_1, N_2, \cdots, N_L$ multi-dimensional DCT. Here, ψ_N represents the transformation matrix of one-dimensional DCT; $\otimes$ represents the Kronecker product, then the three-dimensional DCT dictionary corresponding to the three-dimensional image block of $\sqrt{n} \times \sqrt{n} \times w_Z$ can be described as:

$$\psi_{\tau \times p} = f \otimes \psi_{\sqrt{n} \times \sqrt{k}} \otimes \psi_{w_z \times \sqrt{k}} \quad (5)$$

where $\psi_{\tau \times p}$ is a complete dictionary; w_z is the number of blocks constituting the z-th group of TOFD images.

According to the above analysis, the TOFD image denoising process based on hyperspectral sensor is as follows:

(1) Initialize processing: $z = 1$.

(2) Divide the FD image three-dimensional squares S_Z to obtain the small blocks of $\sqrt{n} \times \sqrt{n} \times w_Z$; sort the small blocks to obtain the column vector of $\tau \times 1$ and then construct the matrix $B_{\tau \times M}$.

(3) Solve the sparse coefficient matrix A on the basis of dictionary $\psi_{\tau \times p}$ and matrix $B_{\tau \times M}$ through the orthogonal matching pursuit algorithm, and perform the following process:

1) Let $E_{err} = \tau\sigma_n^2, A = \phi,\ S = \phi,\ \Lambda = \phi,\ i = 1,\ r = x$;

2) Find index Λ_i to satisfy the following formula:

$$\Lambda_i = \underset{j=1,2,\cdots,K}{\arg\max} |r, \psi_i| \quad (6)$$

3) Let $\Lambda(i) = \Lambda_i, \psi_i = \psi[\Lambda(1,i)]$, find the least square solution $\hat{S}$ of $x = \psi_i \hat{S}$ by the following formula:

$$\hat{S} = \arg\min_S |x - \psi_i S \Vdash (\psi_i^T \psi_i)^{-1} \psi_i^T x \quad (7)$$

4) Set the residual r and update it by the following formula:

$$r = x - \psi_i \hat{S} \quad (8)$$

5) When E_{err} is greater than r, terminate the iteration; if it is reversed, iterate again.

(4) When Λ is not zero, set $A(\Lambda, k_n) = \hat{S}$. k_n is increased by 1, and determine whether M is less than k_n. If the above conditions are met, terminate the iteration; if the above conditions are not met, return to step (3).

(5) Based on the approximate sparse matrix A, update the matrix B using the following formula:

$$B = \psi_{\tau \times p} \times A \quad (9)$$

(6) Replace each column of matrix B with a small image stereo cube of $\sqrt{n} \times \sqrt{n} \times w$.

(7) Merge the image blocks, and average the overlapping image blocks to obtain the TOFD image cube $\hat{S}_Z$ after denoising.

(8) z increases by 1, when z is less than or equal to $Z_{\max}$, return to step (2); When z is greater than $Z_{\max}$, stop the iteration.

Performed in the sequence above, these steps can achieve effective denoising in TOFD images, which helps to improve the accuracy of image defect recognition.

2.3 Implementation of TOFD Image Defect Recognition Based on HSV Block Color Histogram

Based on the results of TOFD image denoising, the HSV block color histogram is used to identify TOFD image defects. HSV is a color space created based on the intuitive characteristics of colors, which consists of hue (H), saturation (S), and brightness (V). Among them, the V component is image brightness information, and the H and S components are related to human visual color perception. In the HSV color space, when the color of an image changes, the H component remains basically unchanged before and after the change, while the S component undergoes a greater change, and the amount of information is much greater in an image with rich colors than in an image with dark colors. When multiplicative noise or additive noise is introduced into the image, the V component in the image will change with the value of the S component under the condition of color constancy, and a large amount of information is concentrated on the component, resulting in a great increase in its information content (Keming et al., 2018). In this paper, the information entropy of the S component in the TOFD image is normalized and defined as the color restoration coefficient of the image, and is expressed as:

$$L = \sum_i^n X_i(k) - B \times \delta[X^0(n) - X^0(1)] \quad (10)$$

where $X_i(k)$ is the distribution probability of the number of pixels of the gray level; δ is the normalization factor.

It is reasonable to use the histogram similarity to measure the color shift degree of the TOFD image. Therefore, in the image S component plane (Jeong et al., 2020), the similarity coefficient J can be used to compare the TOFD image histogram before and after denoising:

$$J = \frac{K_i}{S}(u_{ij} - u_{mn}) \times L \tag{11}$$

where u_{ij} is the S component of the TOFD image before denoising; u_{mn} is the S component of the TOFD image after denoising. Under normal circumstances, the larger the value of J, the higher is the color reproduction of the TOFD image, which is more conducive to the recognition of defects in the TOFD image.

The traditional method of detecting defects in TOFD images usually involves three modules: feature design, feature selection and pattern recognition. The features used are mainly manual low-level features such as geometric features indicating the shape and direction of defects and the texture features of images (Udomkun et al., 2019). Aft er image segmentation, the candidate defect block is obtained, and then their geometric features are extracted (Nodari et al., 2012; Tan and Zhao, 2020); finally, it is determined whether the image block is a defect (Chojka et al., 2020). The geometric features used include area, major axis length, minor axis length, eccentricity, circumference, convex image area, direction, etc. Among them, the eccentricity refers to the eccentricity of an ellipse having the same second moment as the target area, and the direction refers to the angle between the long axis of the ellipse and the x-axis. Obviously, these features describe the shape and direction of the defect and are suitable for defect identification. However, this method is based on feature-based defect recognition, which relies on human experience for accuracy.

There are certain limitations in practical applications. First, it is difficult to know the features that are good features, and the manual design of features is a time-consuming and labor-intensive task, and difficult to complete online. Secondly, in order to shorten the time of image recognition, it also usually selects certain features and fuses them. However, this feature selection is tricky because it involves a priori selection of dimensions. Finally, the three modules mentioned above cannot be optimized jointly (Rahman et al., 2020). Although the TOFD image denoising method based on hyperspectral sensors mentioned in section 1.2 can improve the accuracy of image defect recognition to a certain extent, its recognition accuracy still has room for improvement. For this reason, a TOFD image defect recognition model based on the HSV block color histogram is constructed, which has significant advantages in dealing with problems related to image defect recognition (Son et al., 2019).

A TOFD image defect recognition model based on the HSV block color histogram is constructed by firstly analyzing the HSV block color histogram (Bern et al., 2018). This model is used to initiate the TOFD image defect recognition process:

$$P_n = \min B\{A_c, A_q\} - R_d \times J \tag{12}$$

where A_c is the probability of each gray value; A_q is the background area of the image; R_d is the boundary ofthe image defect.

When using the model shown in Equation (12) to identify defects in a TOFD image, it is necessary to determine the size of the boundary of the non-defective part of the image, and calculate this with Equation (13):

$$G_{sc} = G_0 + \frac{a_1 P_n}{(c_s - \Gamma)(1 + D/D_0)} \tag{13}$$

where G_{sc} is the edge information of the image; G_0 is the size of the image block; Γ is the color set of the image; D is the image space range; D_0 and a_1 are constant.

Combine Equation (12) and Equation (13) to locate the image defect position:

$$G_s = G_{sc} G(\psi_1) G(\psi_s) \tag{14}$$

where $G(\psi_1)$ is the feature of minimizing in-class defects, and the calculation formula of $G(\psi_1)$ is:

$$G(\psi_1) = 1 - \left| \frac{\psi_1}{b_1} \right|^{b_2} \tag{15}$$

where b_1 and b_2 are constants.

Position $G(\psi_s)$ by fitting the empirical formula:

$$G(\psi_s) = a + b \exp(\psi_s) \tag{16}$$

According to the calculation result of Equation (16), the recognition of TOFD image defects is realized. Figure 1 depicts the flow of TOFD image defect recognition process.

3. EXPERIMENTAL VERIFICATION

In order to confirm the effectiveness of the designed TOFD image defect recognition method based on HSV block color histogram, the proposed method, the method of Dai et al. (2018) and the method of Itakura and Hosoi (2020) were used for testing.

3.1 Experimental Environment and Parameter Settings

A total of 300 samples of different types of defect images were collected as input. In order to prevent problems caused by sample imbalance, the image size of all images was the same (100 mm $\times$100 mm). The three methods were loaded on a virtual simulation platform, the specific parameters of which are shown in Table 1.

3.2 Experimental Results and Analysis

For comparison, the test results achieved by the three methods applied to determine defect recognition accuracy are presented in Figure 2.

An analysis of Figure 2 shows that with multiple iterations, the recognition accuracy of the TOFD image defect recognition method based on HSV block color histogram is higher than that of the image recognition method based on the low

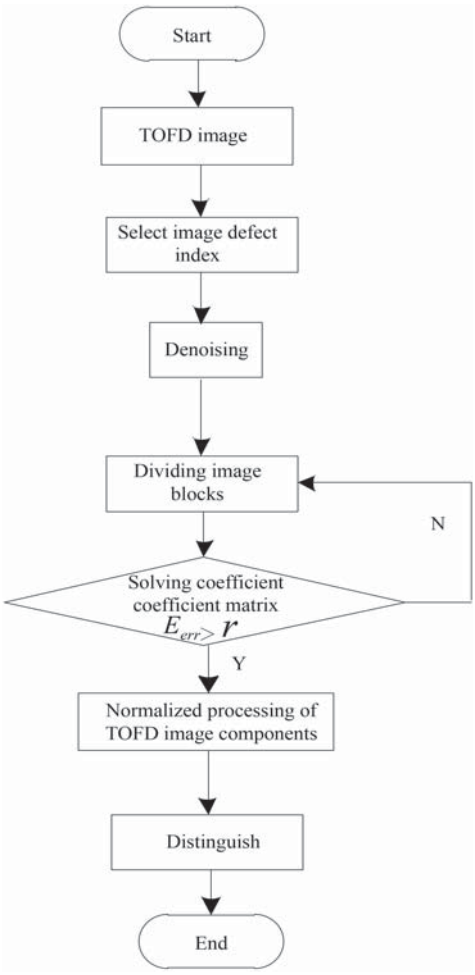

Figure 1 TOFD image defect recognition process.

Table 1 Computer virtual simulation platform parameters.

Name	Specific parameters
CPU	Intel i9,3.75 GHz
Hard disk 1T SSD	
Graphics card	NVIDIA
RAM	32 G
Operating system	Windows 10

space complexity codebook used for image similarity, and the recognition accuracy of the image recognition method. The proposed method achieved an accuracy up to 85%, much higher than that of the traditional methods. This is because the proposed method selects TOFD image defect indicators based on the shape and gray difference of various defects in the actual image, and uses a hyperspectral sensor to denoise the TOFD image with defect indicators to reduce noise and accurately identify Defects, thereby improving the accuracy ofthe simulation.

In order to further confirm the effectiveness of the designed method, the image defect recognition time is used as the test index to compare different methods. Figure 3 shows the results and facilitates comparison.

From Figure 3, it can be seen that the identification time required by the proposed method, and that required by the Shinomiya and Hoshino (2019) method and the Chakraborty et al. (2018) method, fluctuates under different iteration times, although the proposed method requires less time overall. This is because the method uses hyperspectral sensors to denoise the TOFD image with defect indicators, eliminates the noise in the image, simplifies the complexity of image recognition, and reduces the time required to recognise defects.

In addition to image defect recognition accuracy and recognition time, the number of defect recognitions is also one of the indicators used to confirm the effectiveness of the proposed method. Therefore, the number of defect recognitions is used as an indicator to compare the recognition effects of different methods. The results are shown in Figure 4. Figure 4(a) shows the recognition results when the image is 100; Figure 4(b) shows the recognition results when the image is 200; Figure 4(c) shows the recognition results when the image is 300.

According to the recognition results shown in Figure 4, the number of recognitions of defects in TOFD images based on HSV block color histogram is always higher than

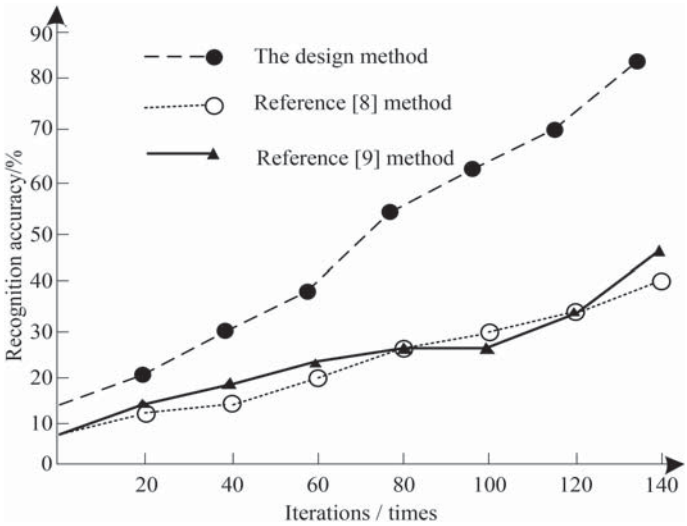

Figure 2 The recognition accuracy of different methods.

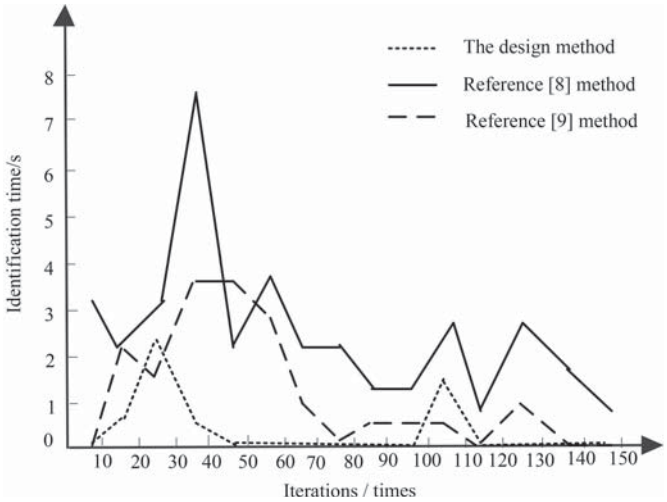

Figure 3 Comparison of recognition time required by different methods.

those based on low spatial complexity codebook and image similarity and image recognition methods even when the number of images varies. It shows that the propose method can identify more defects. The identification result is more comprehensive, and the reliability of identification test results is greater. This is because the method applies an image defect recognition model based on HSV block color histogram according to the denoising results. The model can obtain the image defect information, make the defect recognition more comprehensive, and improve the coverage of the recognition results.

The experiments above confirm the effectiveness of the proposed method. In order to visually display the effect of the designed method on TOFD image defect recognition, and to more intuitively display the application value of the design method, different methods are used to obtain the image defect recognition effect, as shown in Figure 5.

Figure 5 shows that, among the complex images with defects, the color of the image obtained by the method of Dai et al. (2018) is relatively single, and the defect characteristics of the image cannot be clearly described, which shows that the method cannot provide reliable support for image processing. In contrast, the color saturation of the image obtained by the proposed method is greater, and therefore highlights the defect features more clearly. The value of this method is confirmed since its application yields better results for defect recognition.

4. DISCUSSION

In order to reduce the errors that occur as a result of manual recognition, and to recognize image defects more objectively, reliably, efficiently and intelligently, research on computer-based automatic recognition methods of image defects has become a new trend and important direction. The premise of computer-based recognition is to obtain digitized images through a dedicated scanner or CCD camera. Then image processing technology is used to preprocess the digitized image and coarsely locate the defect area. The characteristics of defects are extracted based on professional knowledge or experience, and finally machine learning and other related

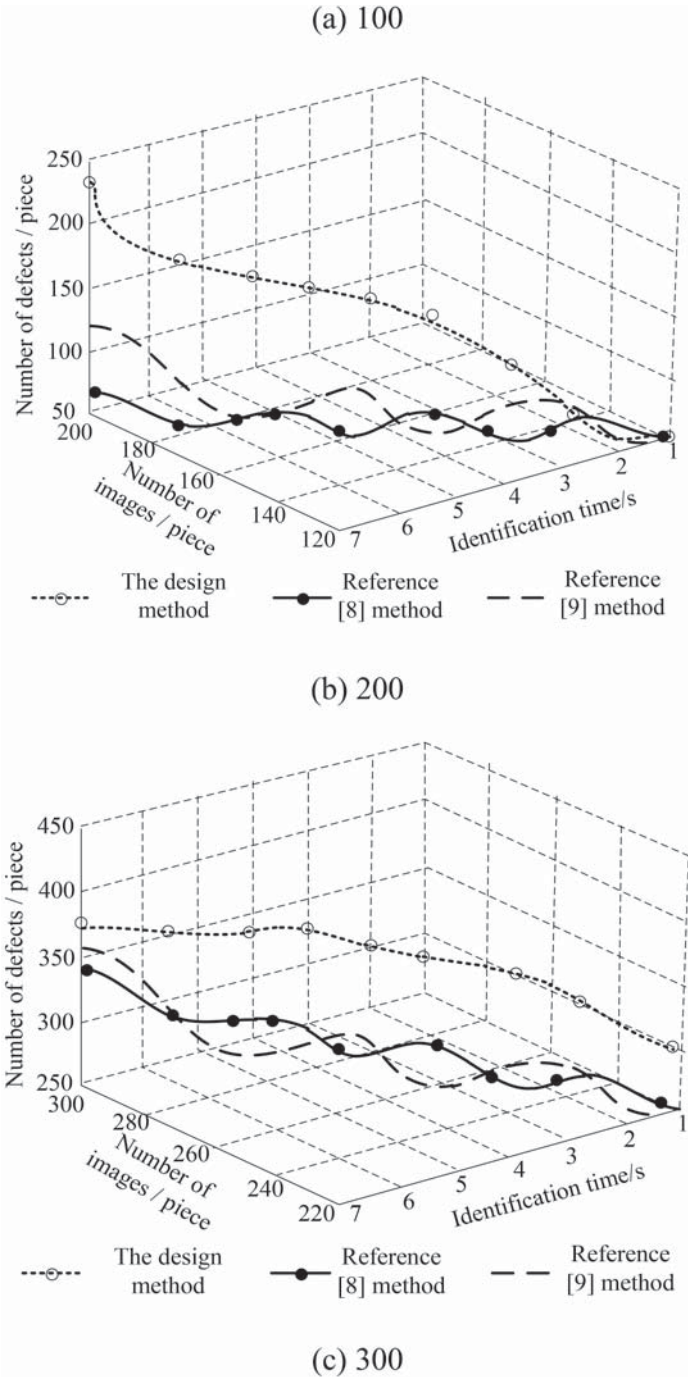

Figure 4 Comparison of the number of defects identified by different methods.

algorithms are applied to achieve classification. Automatic computerized recognition can overcome the influence of subjective or environmental factors, thereby obtaining more reliable and accurate recognition results, with greater recognition efficiency than is obtained by the manual method. Hence, an increasing number of scholars are conducting research on automatic, computer-based identification systems. However, most of these systems are operated interactively manually, and require manual intervention. The machine-learning-based classifier involved in such recognition systems cannot directly extract representative features from the original image.

Therefore, it is necessary to manually design features such as geometric size, texture, grayscale, directional gradient histogram, and local binary pattern features. In order to extract these features, researchers need to understand the image processing and defect formation mechanisms in advance, which requires manual intervention. Therefore, it is impossible to realize automatic recognition in a true sense.

The recognition of defects in TOFD images depends on the operator's data analysis experience and knowledge. Moreover, human factors (operator's experience, level of expertise, and fatigue) have a greater impact on the recognition results, and misjudgments and omissions oft en occur. Poor judgement and inconsistencies, etc., reduce the reliability of defect identification. The effective recognition of TOFD image defects and the improvement of recognition accuracy is

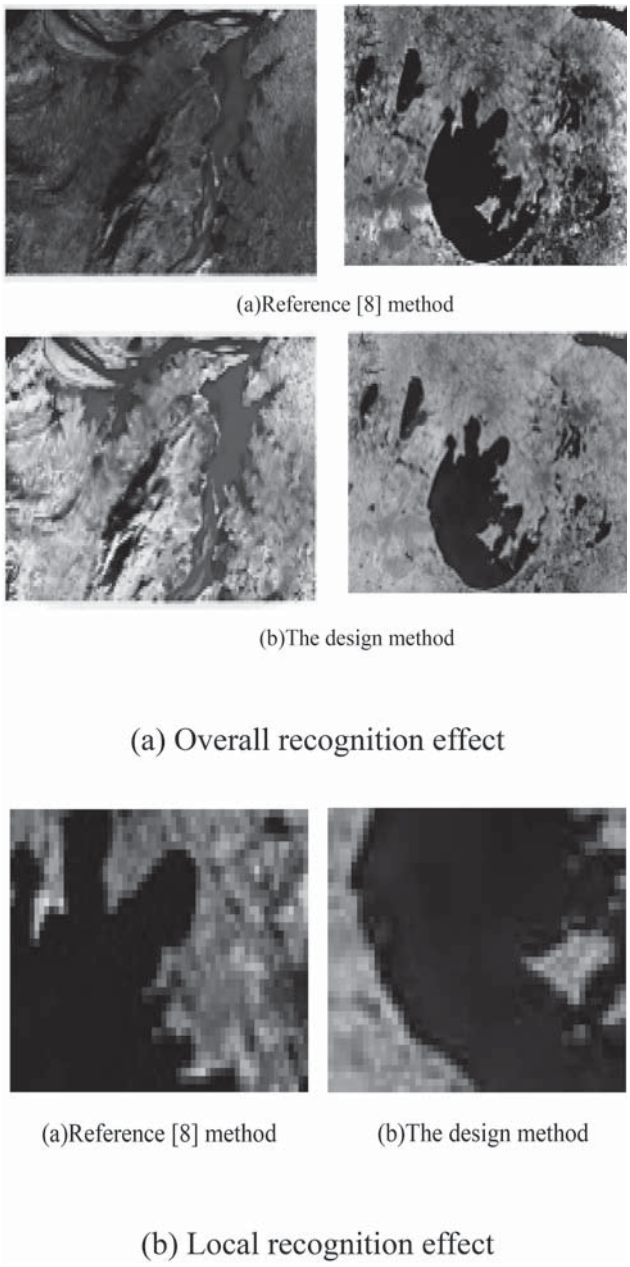

Figure 5 Comparison of recognition effect.

a research hotspot in the field of image processing locally and globally, with the potential for wide commercial application. This paper proposes and evaluates a TOFD image defect recognition method based on HSV block color histogram. The main research steps of this paper are as follows:

(1) First, we select TOFD image defect indicators: average gray background ratio, defective perimeter area ratio, and defective symmetry.

(2) Then, based on these indicators, a hyperspectral sensor is used to denoise the TOFD image with defective indicators.

(3) Finally, a model for the effective recognition of image defects is established based on the HSV block color histogram.

(4) Establish test samples and carry out experimental verification.

The experimental results show that this method successfully addresses the shortcomings of the current methods used for defect image recognition, and significantly improves image recognition.

5. CONCLUSIONS

In order to utilize the recognition results to improve the image processing effect, provide more comprehensive image defect information, and improve the accuracy of image defect recognition, this paper proposes a TOFD image defect recognition method based on the HSV block color histogram. The experimental results prove that the method can obtain a

large amount of defect information in the specific application process; at the same time, it improves the accuracy of image recognition, reduces the time required for image recognition, and gives this method wider applicability.

At the same time, further research is needed to achieve automatic extraction of defect information in TOFD images. Starting from the practicability of updating the TOFD image database, the recognition result can be input as vector data to the image database, which exploits the complementary advantages of various methods of image processing.

REFERENCES

1. Ali, A., Lee, T.L., Thoe, N.K., Ismail, N., Abu Bakar, S.Z.S., 2019. Transforming Public Libraries into Digital Knowledge Dissemination Centre in Supporting Lifelong Blended Learning Programmes for Rural Youths. *Acta Informatica Malaysia*, 3(1), 16–20.
2. Aljanabi, M.A., Hussain, Z.M., Lu, S.F., 2018. An entropy-histogram approach for image similarity and face recognition. *Mathematical Problems in Engineering*, (8), 1–18.
3. Bern, G, Schoettl, P., Van Rooyen, D.W., Anna, H., 2019. Parallel in-situ measurement of heliostat aim points in central receiver systems by image processing methods. *Solar Energy* 180(3): 648–663.
4. Chakraborty, S., Singh, S.K., Chakraborty, P., 2018. Centre symmetric quadruple pattern: A novel descriptor for facial image recognition and retrieval. *Pattern Recognition Letters*, 115(11), 50–58.
5. Chen, F.P, Qi, J.H., 2019. Rotation-invariant texture features applied in image pattern recognition. *Computer Simulation*, 36(2): 363–366.
6. Chojka, A., Artiemjew, P., Jacek, R., 2020. RFI artefacts detection in sentinel-l level-1 SLC data based on image processing techniques. *Sensors*, 20(10): 2919.
7. Corti, E., Khanna, A., Niang, K., Robertson, J., Moselund, K.E., Gotsmann, M.B., Datta, S., Karg, S., 2020. Time-delay encoded image recognition in a network of resistively coupled VO on Si oscillators. *IEEE Electron Device Letters*, 41(4), 629–632.
8. Dai W., Pu R., Tang C., 2018. Factors Aff ecting "A" Luxury Brand Loyalty on Chinese College Students in Shanghai City of China. *Inormation Management and Computer* 41(3), 14–17.
9. Itakura, K., Hosoi, F. 2020, Automatic method for segmenting leaves by combining 2D and 3D image-processing techniques. *Applied Optics*, 59(2), 545.
10. Jang, S.W., Ahn, B., 2020. Implementation of Detection System for drowsy driving prevention using image recognition and IoT. *Sustainability* 12(7), 3037.
11. Jeong, H., Kwon, GR., Lee, S.W., 2020. Deterioration diagnosis of solar module using thermal and visible image processing. *Energies*, 13(11): 2856.
12. Kas, M., El Merabet, Y., Ruichek, Y., Messoussia, R., 2018. Mixed neighborhood topology cross decoded patterns for image-based face recognition. *Expert Systems with Applications*, 114(12), 119–142.
13. Keming, M., Duo, L., Dazhi, E., Zhenhua, T., 2018. A case study on attribute recognition of heated metal mark image using deep convolutional neural networks. *Sensors*, 18(6): 1871.
14. Kropp, C., Koch, C., Knig, M., 2018. Interior construction state recognition with 4D BIM registered image sequences. *Automation in Construction*, 86(2), 11–32.
15. Nodari, A., Gallo, I., Vanetti, M., Albertini, S., 2012. Color and texture indexing using an object segmentation approach. *Engineering Intelligent Systems*, 20(1-2), 47–57.
16. Quionez, Y., Lizarraga, C., Peraza, J., Oscar, Z., 2020. Image recognition in UAV videos using convolutional neural networks. *IETSofnv are*, 14(2), 176–181.
17. Rahman, M.O., Hussain, A., Basri, H., 2020. Automated sorting of recycled paper using smart image processing. *Automatisierungstechnik*, 68(4): 277–293.
18. Sharan, R.V, Moir, T.J., 2018. Pseudo-color cochleagram image feature and sequential feature selection for robust acoustic event recognition. *Applied Acoustics*, 140(11): 198–204.
19. Shinomiya, Y., Hoshino, YA., 2019. Feature encoding based on low space complexity codebook called fuzzy codebook for image recognition. *International Journal of Fuzzy Systems*, 21(1), 274–280.
20. Shota, S., Toshiya, W., Susumu, S., Masaru, K., 2018. Multi-touch tabletop system using infr ared image recognition for user position identification. *Sensors*, 18(5), 1559.
21. Simone, M., Emanuela, F., Valerio, S., Ernesto, A., Joaquin, D.R.F., Jacopo, A., 2018. Tracking fish abundance by underwater image recognition. *Scientific Reports*, 8(1), 13748.
22. Singh, O.P, Kumar, G, Kumar, M., 2019. Role of Taguchi and Grey Relational Method in Optimization of Machining Parameters of Different Materials: A Review. *Acta Electronica Malaysia*, 3(1), 19–22.
23. Son, J., Mandracchia, B., Caponegro, M.D., Stella, T., 2019. BSSE: An open-source image processing tool for miniaturized microscopy. *Optics Express*, 27(13): 17620.
24. Tan, Y.L., Zhao, Y.Q., 2020. A gray level-gradient-based two-dimensional (2D) otsu thresholding method for image segmentation. *Engineering Intelligent Systems*, 28(2), 109–113.
25. Udomkun, P., Innawong, B., Sopa, W., 2019. Can the image processing technique be potentially used to evaluate quality of fr ying oil? *Journal ofFood Quality* (1): 1–12.
26. Umer, S., Dhara, B.C., Chanda, B., 2019. NIR and VW iris image recognition using ensemble ofpatch statistics features. *The Visual Computer* 35(9), 1327–1344.